Solidum Petit In Profundis · Universitetas Aarhusiensis

Growing Single-Layer Niobium Disulphide on Bilayer Graphene

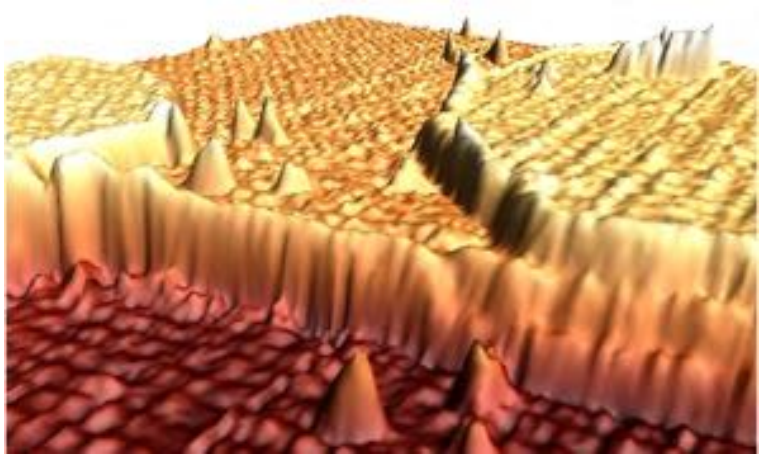

Written By:

Christian Valentiner-Branth Nielsen

Student number: 201906552

Supervised by:

Jill Miwa

Bachelor's thesis

Spring 2022

Abstract

Transition metal dichalcogenides (TMDCs) are interesting materials due to their unique optical and electronic properties. They are layered van der Waals solids, and like graphite they can be taken to the single layer (SL) limit where they might show new properties, which can be tuned by the choice of substrate, and perhaps by growth method. Among the TMDCs NbS_2 stands out as unique, due to being superconducting without a charge density wave (CDW). Therefore it is interesting to grow SL NbS_2 on different substrates using different methods. The purpose of this thesis is to attempt to grow SL NbS_2 on bilayer graphene (BLG) on SiC(0001) by evaporation of Nb onto the substrate in a dimethyl disulphide (DMDS) atmosphere, followed by an anneal. To characterise the different surfaces along the way, scanning tunneling microscopy (STM) is used.

SL NbS_2 was first successfully grown on Au(111), and the results agree with previously published work. Growth attempts were then made on highly oriented pyrolytic graphite to adjust the evaporation parameters. Finally, an attempt was made to grow SL NbS_2 on BLG on SiC(0001). This resulted in well-formed, flat islands, most likely consisting of some sort of intercalated material. This material may be some form of NbS_2.

Resúme

Overgangsmetal dichalcogenider (TMDC'er) er interessante materialer på grund af deres unikke optiske og elektroniske egenskaber. De er lagdelte van der Waals materialer, og ligesom grafit, kan de tages til enkeltlagsgrænsen hvor de måske viser nye egenskaber, der kan ændres ved valg af underlag, og måske ved syntese-metode. Blandt TMDC'erne er NbS_2 unik, da den er superledende uden at vise en charge density wave. Derfor er det interessant at syntetisere enkeltlags NbS_2 på forskellige underlag. Formålet med denne afhandling er at forsøge at syntetisere enkeltlags NbS_2 på bi-lags grafen (BLG) på SiC(0001) ved at fordampe Nb ned på underlaget i en atmosfære af dimethyl disulphid, efterfulgt af en opvarmning. For at karakterisere de forskellige overflader undervejs, anvendes skanning tunnel mikroskopi (STM).

Enkeltlags NbS_2 blev først syntetiseret på Au(111). Resultaterne stemmer overens med tidligere udgivet forskning. Der blev også gjort syntese-forsøg på meget orienteret pyrolytisk grafit (HOPG) for at justere fordampningsparametrene. Til sidst blev der gjort et forsøg på at syntetisere enkeltlags NbS_2 på BLG på SiC(0001). Dette resulterede i nogle velformede, flade øer, der højst sandsynligt består af en eller anden form for materiale der har lagt sig under grafenen. Dette materiale er muligvis en eller anden form for NbS_2.

Preface

This is my bachelors thesis, submitted to the Department of Physics and Astronomy at Aarhus University in order to fulfill the requirements for a Bachelor's degree in Physics. The work has been performed between 31/1/2022 and 15/6/2022 under the supervision of Associate Professor Jill Miwa, Department of Physics and Astronomy, Aarhus University, 8000 Aarhus C, Denmark.

Front page image: Three-dimensional rendering of STM image showing another view of the product of the attempt to grow single-layer NbS_2 on bilayer graphene on SiC(0001).

Acknowledgements

Most of the experimental work has taken place at the stand-alone chamber for sample preparation and scanning tunneling microscopy in the laboratory, but some has taken place in the SGM3 endstation of the ASTRID2 synchrotron radiation source at the Institute for Storage Ring Facilities in Aarhus, using the STM in there. All the experimental work, including repairing the thermocouple and mounting the bilayer graphene on SiC(0001) substrates, was done by me, except for the mounting of the Au(111) and HOPG substrates, as well as the replacement of the STM, which was done by Marco Bianchi.

I want to thank Jill Miwa, for being an amazing supervisor, always ready to help and answer questions, Marco Bianchi, for his indispensable knowledge of the field and the lab-equipment, without whom this project would have quickly grinded to a halt, Andrea Berti, for lending me STM images of Au(111) taken on the SGM3 STM for calibration purposes, and Miguel Ugeda's group at Donostia International Physics Center (DIPC) for making the bilayer graphene on SiC(0001) substrates used in this thesis.

List of Abbreviations and Acronyms

2D Two-dimensional

AFM Atomic force microscopy

ARPES Angle resolved photoemission spectroscopy

BLG Bilayer graphene

CDW Charge density wave

DMDS Dimethyl disulphide

FFT Fast Fourier transform

HOPG Highly oriented pyrolytic graphite

LDOS Local density of states

LL Load-lock

MC Main chamber

SL Single layer

STM Scanning tunneling microscopy

STS Scanning tunneling spectroscopy

TMDC Transition metal dichalcogenide

UHV Ultra-high vacuum

XPS X-ray photoemission spectroscopy

Contents

1 Introduction

Research in two-dimensional (2D) materials, any material consisting of a single or few atoms thick film, has seen a marked increase in interest ever since the experimental realisation of graphene in 2004. 2D films could potentially be made from any layered material where the layers are only weakly bonded, the so-called van der Waals solids. Under this category lies the transition metal dichalcogenides (TMDCs). In any TMDC, every layer has the general chemical formula MX_2 and consists of a layer of transition metal atoms (M=Mo, W, T, Nb, etc.) placed in between two layers of chalcogen atoms (X=S, Se, Te). Most TMDCs exist in two phases, the trigonal prismatic (1H/2H) phase, where the chalcogenide atoms are right above each other, and the octahedral (1T) phase, where the layers are shifted. The 1T phase is unstable for many TMDCs, and can spontaneously change into the 1H/2H phase, however, this is not the case for all TMDCs. TMDCs show unique electrical and optical properties, such as superconductivity and charge density waves (CDW) and are therefore extremely interesting candidates for novel opto-electrical devices [1–4]. Among these, 2H-NbS_2 stands out as it seemingly displays superconductivity without a CDW, which is unusual for superconducting TMDCs [5–7]. Therefore NbS_2 is of great interest.

As with graphene, the TMDCs can radically change their properties when scaled down to the single layer (SL) limit, where they consist of a single X-M-X layer. An intriguing aspect of the SL limit is the fact that, because of the lower dimensionality, they are extremely sensitive to their surrounding environment. For $NbSe_2$, a material similar to

NbS_2, this was recently made abundantly clear in Ref. [8], showing that the electronic properties can be modified extensively by choice of substrate. It is therefore of great interest to grow high quality SL TMDCs on as many substates as possible. SL NbS_2 has already been grown and studied on Au(111) [9]. Using another method, it has also been grown on bilayer graphene (BLG) on SiC(0001), on which it showed a (3×3) CDW [10], similar to $NbSe_2$ [8]. However much more experimental information is still needed. To obtain that information, it is useful to try to use different methods to synthesise the SL material, as they might give different results [11].

Based on these observations, the aim of this project is to attempt to grow SL NbS_2 on BLG on SiC(0001) substrates, using a method similar to that used for growing NbS_2 on Au(111), as is done in Ref. [9]. To achieve this NbS_2 will first be grown on Au(111), which serves as a great platform for growing large area, high quality samples of SL NbS_2, hence serving as a baseline with which to compare other observations. Then experiments trying to grow SL NbS_2 on highly oriented pyrolytic graphite (HOPG) will be done to tune the growth parameters, as the surface interaction should be similar to the BLG surface, since HOPG is many layers of graphene. Finally, attempts will be made at growing SL NbS_2 on the graphene. The samples will all be inspected with scanning tunneling microscopy (STM) to characterise the surfaces, as this is the ideal tool to characterise the substrates and any grown material all the way down to the atomic limit.

2 Experimental setup and techniques

In this chapter, the experimental setup and techniques will be explained, alongside a mostly phenomenological explanation of the principle of STM.

2.1 Equipment

All experiments were carried out in a home built ultra-high vacuum (UHV) chamber. Figure 1a) and b) give an overview over the chamber and instruments. Figure 1a) shows the instrument controllers and gauges, used to read the pressure inside the chamber for example. Figure 1b) shows the chamber alongside the the different instruments and most of the pumps used. The chamber consists of a main chamber (MC) and a load-lock (LL). The MC is pumped to a base pressure of $\sim 1 \cdot 10^{-10}$ mbar by an external roughing pump, the MC turbo pump, and an ion pump placed beneath the chamber. The LL is a small volume connected to the MC by a VAT valve, which is a valve that can be opened like a gate. The LL is used to introduce samples to the chamber through the VAT valve, and is pumped by another roughing pump and the LL turbo pump.

All the instruments used to interact with the sample are placed within the MC. Inside the MC the sample is held either in the manipulator or the STM. The transfer arms are used to move the sample out of the LL and between the manipulator and STM. The manipulator is a column with a vertical sample holder at the end. Via the manipulator, the sample's position (x, y, z and angle) can be accu-

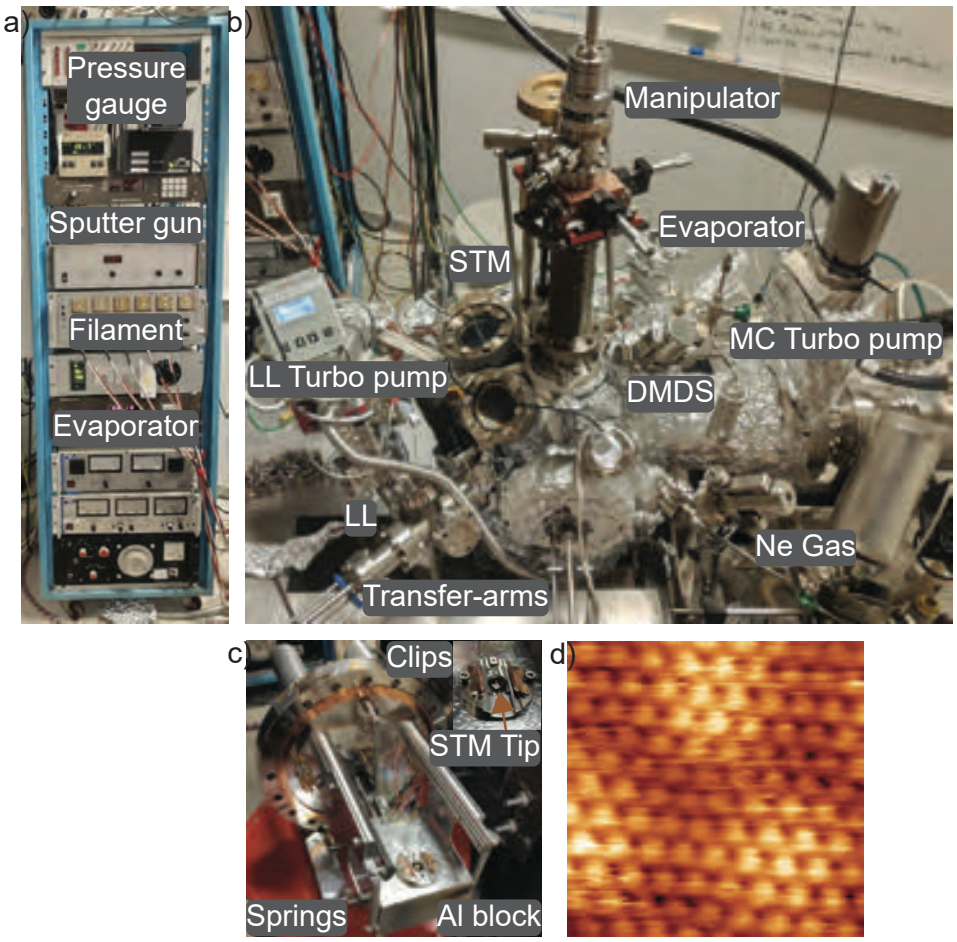

Figure 1: a) The instrument column with all the controllers and gauges. b) An overview of the main chamber, described in the text. The STM is on the back on the chamber. c) The STM as it is outside the chamber. Inset: A close up of the sample holder in the STM showing the tip and the clips that hold the sample plate. d) A (30×30) Å^2 atomically resolved STM image of NbS_2 on Au(111). Image parameters: $V_b = 220.9\,\text{mV}$ and $I_t = 0.70\,\text{nA}$.

rately controlled. Behind the sample holder on the manipulator is a filament for annealing. The temperature of the sample can be monitored via a thermocouple that is connected by placing the sample in the manipulator. The Ne gas (ALPHAGAZ) and dimethyl disulphide (DMDS, with $> 99\%$ purity, Sigma-Aldrich) can be introduced to the chamber quite precisely via precision leak valves. The Ne gas is used for sputtering with a sputter gun (the controller is shown on figure 1a)), and the DMDS is used for growth. A commercial electron-beam evaporator is used for depositing metal onto the sample. To control the amount of material deposited, the so-called emission current (I_{em}) was adjusted (all other evaporator parameters were kept mostly constant (high voltage $V_H = 1.5\,\mathrm{kV}$ and filament current $I_{fil} = 3.6\,\mathrm{A}$)). Figure 1c) shows the Aarhus STM used, as it is outside the chamber. The Al block holds the main parts of the STM, and can be released such that is hangs freely in the springs when scanning. The springs ensure good vibrational isolation, and the clips used to hold the sample ensure that the sample does not move or shake during scanning. Both of these components are important for reducing noise in the STM images.

2.2 Substrates

The term substrate refers to the base material on which processes are conducted, such as growth. These are referred to by the compound followed by the cut of the surface in parentheses (if relevant). The cut is designated by the Miller indices which denote a plane orthogonal to the reciprocal lattice vector given by the indices and the basis of

the reciprocal lattice [12]. Three types of substrates are used in this thesis. Au(111) crystals (MaTeck), HOPG crystals (SPI), and BLG on SiC(0001) substrates. Au(111) crystals are useful substrates for synthesis of SL TMDCs because of the reactive herringbone reconstruction of the (111) surface [9]. HOPG is useful since it consists of many layers of graphene. Hence the surface interaction should be similar to graphene, and it can therefore act as a more reusable testing surface. BLG on SiC(0001) substrates are two layers of graphene on top on a SiC(0001) crystal and it is quite interesting system in itself. As mentioned SL TMDCs grown on this substrate can show radically different properties compared to Au(111), and finding ways to prepare high quality samples on this substrate is therefore very interesting.

2.3 Sputtering and Annealing

A prerequisite for surface science in UHV is cleanliness, even at the atomic level [9]. In this thesis, two methods of cleaning are used, based on the techniques of sputtering and annealing. The Au(111) samples are cleaned via a sputter and anneal cycle. The sputtering constitutes a process in which the sample is bombarded with inert gas ions, here Ne^+, by using a sputter gun, eroding the contaminants adsorbed to the surface. This leaves the surface quite rough however [13], so the sample is then annealed.

Annealing is a heat treatment in which the sample is heated slowly to a certain temperature, kept there and then cooled down slowly again. This is done by passing a high current through the annealing filament in the manipulator, thus irradiating the sample, which heats

it up. Annealing allows metallic surfaces to reconstruct themselves by adding the thermal energy to let atoms migrate in the lattice, reducing the number of defects and stress on the surface. By cooling the crystal down slowly, the appropriate lattices form. This at the least works for the Au(111) surface [14]. Annealing can also be used to add thermal energy for other purposes. Non-metallic samples are cleaned by annealing as this adds the thermal energy needed to desorb many of the adsorbates attached to the surface [9].

2.4 Synthesis of NbS_2

After cleaning the substrate, synthesis of SL NbS_2 can be be attempted. The general procedure followed here is also used to grow other SL TMDCs [9, 11, 15, 16]. This is done by evaporating high purity Nb (99.9% purity, Goodfellow) onto the substrate surface, while maintaining an atmosphere of DMDS ($C_2H_6S_2$), which acts as the sulphur source. The sample is then annealed keeping the same pressure of DMDS. Inspired by the work in Ref. [16], the DMDS valve is closed at 250 °C.

2.5 Scanning Tunneling Microscopy

As the name suggests scanning tunneling microscopy uses the quantum mechanical phenomena of tunneling to take pictures of very small areas [17]. More precisely, it uses an extremely pointy needle (shown in the inset of figure 1c)), made of some transition metal or alloy (typically W or Pt-Ir), where the tip of the needle can be approximated

as a single atom. In the STM used, the tip is a Pt-Ir alloy (ratio 80-20). By applying a bias voltage (V_b) between sample and tip, a tunneling current (I_t) can flow when the electronic wavefunctions of sample and tip overlap sufficiently. This tunneling current has an exponential relationship to the relative tip-sample distance, which is as follows. The tunneling conductance, G, is given from the constant conductance quantum $G_0 = 77.48\,\mu$S, the decay constant κ depending on the surface work function (the energy required to remove an electron from the surface), and the relative tip-sample distance $z - z_e$, where z_e is the tip-sample equilibrium distance i.e., the distance where the tip is in one atom contact with the sample [18]:

$$G(z) = G_0 e^{-2\kappa(z-z_e)}. \tag{1}$$

This exponential relation is extremely important as a small change in height becomes a much larger change in current, which can be detected much more easily than the microscopic changes in height on the surface.

There are two basic ways to do STM. Both involve raster scanning the tip across the surface using piezoelectric crystals as drivers, and measuring the tunneling current. There is constant height mode, where the tip is kept at a constant height and only the current is measured. Then there is the method used in this project, constant current mode, where the height is measured while keeping the tunneling current constant via a feedback circuit. If the tip gets too close to the surface, the current becomes too high and the tip is pulled back and vice versa [18]. This mode is used since it is safer, as the feedback loop helps the tip not crash into the surface, and this mode provides more

direct height measurements. An example of an STM image acquired using constant current mode is shown in figure 1d).

It is important to keep in mind that since the tunneling current is a product of overlapping wavefunctions, the images produced are convolutions of topography and electronic structure. More precisely, the images are convolutions of the surface topography and the local density of states (LDOS) [19]. The quantum mechanical nature of STM also means that the tip state is of great importance. Spontaneous tip state changes may suddenly change the image, for example whether or not you have atomic resolution at any given time. Another phenomenon to be aware of while analysing STM images is corrugation inversion, where what previously looked like protrusions before can suddenly become depressions or the other way around [18].

In summary, by measuring the height as the tip scans along the surface, an image of said surface is generated. From these images a great deal of information can be gained, such as apparent height and distances in the xy plane.

3 Results

Here the results of the experiments carried out are presented. Firstly, a structural characterisation of NbS_2 on Au(111) will be presented. Next, the progress made by experimenting on HOPG will be accounted for. Finally, the structure of the attempt at growing NbS_2 on BLG on SiC(0001) will be analysed.

All STM images are calibrated with the WSxM software [20], according to which STM was used for the respective images. All analysis is also carried out using said software. Beyond the statistical errors quoted here, there is an additional error of 10-15% due to piezo creep and thermal drift. With the color scale chosen, higher points in the images are lighter, and low points are darker.

3.1 NbS_2 on Au(111)

First, NbS_2 was grown on an Au(111) substrate. The substrate was cleaned using two cycles of sputtering using Ne^+ ions, with the Ne gas pressure at $\sim 2.5 \cdot 10^{-6}$ mbar. A cycle consists of sputtering at three angles, for 10 minutes each. Two times at 30 degrees from normal incidence, to both sides, and once at normal incidence. The first cycle is done with the ion energy at 1.5 keV and the next is done with 0.5 keV. Lastly, the substrate is annealed to 700 °C for 20 minutes. This was usually sufficient to bring out the characteristic herringbone reconstruction [21, 22], which indicates that the surface is clean enough [9]. An example of this herringbone can be seen 2a). If this was not enough one can sputter the substrate some more at ion energy 0.5 keV

and anneal the substrate again.

NbS_2 was synthesised on the Au(111) substrate by evaporating Nb for 10 minutes ($I_{em} = 30\,\text{mA}$) with $\sim 2 \cdot 10^{-6}\,\text{mbar}$ DMDS pressure, and a $\sim 450\,^{\circ}\text{C}$ anneal for 30 minutes. It should now be mentioned that after the growth, it was discovered that the STM used up until this point was broken. The repair could not be made in vacuum, so the chamber had to be vented. Luckily the sample could be transferred in air to another UHV chamber, which also had an STM. This is where the images of NbS_2 on Au(111) were taken. After taking out the old STM, a new STM was installed.

The resulting images reveal several islands. Figure 2b) shows the largest island found, on which a hexagonal superstructure can be seen. On this island atomic resolution was achieved, as shown in figure 2c), also showing the hexagonal superstructure in more detail. The irregular structure surrounding the island in figure 2b) is most likely due to the transfer in air, but it might be unordered Nb or S, left over from the growth. As shown in figure 2d) the hexagonal superstructure seen in figure 2b) and c) can be explained as being a moiré pattern generated by overlapping the hexagonal lattices of NbS_2 and Au(111). This is also shown in Ref. [9] and was partly used to identify islands of NbS_2. A moiré pattern is a completely general effect caused by placing any two lattices on top of each other, that are distorted relative to each other in some way, be it a different lattice constant, structure or relative rotation [23].

From line profiles such as shown in 2e) the lattice constant of the moiré or atomic lattice, can be determined by averaging the distance

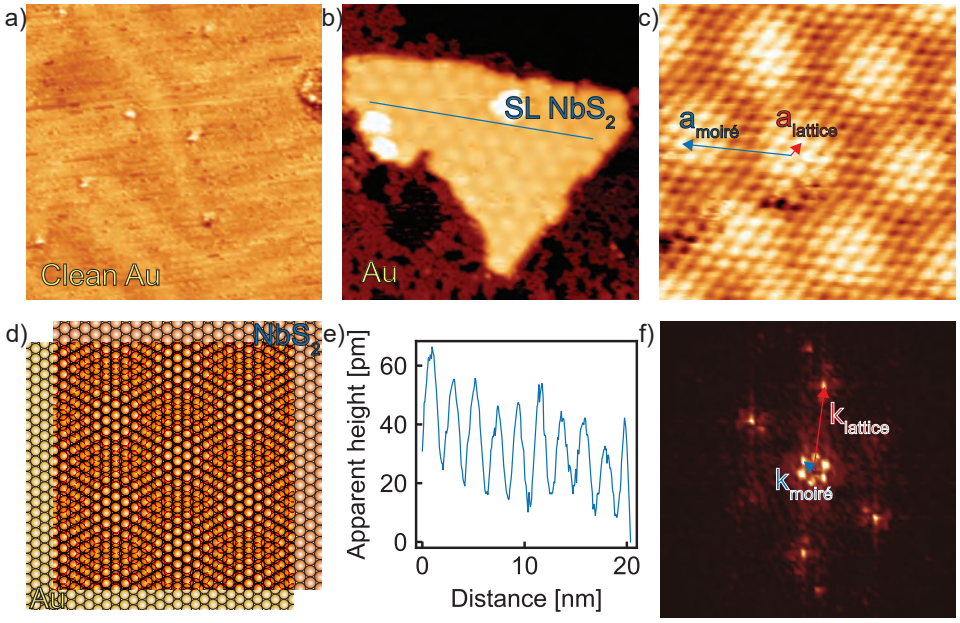

Figure 2: a) A (254×254) Å^2 image of the clean Au(111) surface, showing the distinctive herringbone reconstruction. The distortions in the herringbone is due to pinning by impurities or defects, which are the bright spots. Image parameters: $V_b = -441.9\,\text{mV}$ and $I_t = -0.54\,\text{nA}$. b) A (254×254) Å^2 image showing an island of SL NbS_2. Note the hexagonal moiré pattern. The color scale has been adjusted to show the moiré most effectively, which is why the top right corner is black. Image parameters: $V_b = 625.0\,\text{mV}$ and $I_t = 0.44\,\text{nA}$ c) A (58×58) Å^2 atomically resolved STM image, showing the hexagonal structure of both the atomic lattice and the moiré pattern. The dark spots are defects in the atomic lattice e.g. missing atoms. Note also the oval atoms, clearly seen in the top left of the corner. Image parameters: $V_b = 262.8\,\text{mV}$ and $I_t = 0.59\,\text{nA}$. d) This schematic shows how overlapping the hexagonal lattices of the NbS_2 and Au(111) surface results in a hexagonal moiré. e) A line profile taken from the blue line in panel b) showing the periodic change in apparent height due to the moiré. f) The FFT of the image in panel c), showing the spots due to the atomic lattice, and moiré. Note that some of the spots are less intense.

between peaks. Such line profiles can also be used to measure differences in apparent height, as will be shown later. However, as the height is a product of tip state, topography and LDOS, these are not absolute height measurements, hence the term 'apparent height'. Another method involves taking the fast Fourier transform (FFT) of the images, where any periodicities in the image will shown up as bright spots. The FFT of an image such as 2c), which shows both the atoms and moiré, will correspondingly have spots representing both the atoms and moiré depending on the resolution. This is clearly shown in figure 2f). This can also be used to measure other superstructures, where the structure is not immediately recognisable. As it is a Fourier transform, the FFT of a 'real space' image represents the reciprocal space and as such, short range effects like atoms are far from the center and long range effects such as the moiré are closer to the center. Note also, that in real images, the atoms are not always perfectly round, such as the oval atoms of parts of figure 2c). This results in the spots having different intensities in different directions, such as the weak spots in figure 2f), the axis of which aligns with where the atoms of figure 2c) are stretched. To obtain information from the FFTs one measures the distance from the center in reciprocal space, k. Normally one would just take the reciprocal value to get the real space value, a, but because of limitations in the software used, the value has to be corrected by a factor. For a hexagonal lattice, the conversion is made with the following expression:

$$a = \left(\frac{\sqrt{3}}{2}k\right)^{-1} \tag{2}$$

Hence, by measuring the intense spots in the FFTs of different

atomically resolved images of NbS_2 on Au(111) and taking the mean, the atomic lattice constant is measured to be 3.38 ± 0.06 Å, where the error is just the error in the mean. The moiré pattern is measured using figure 2b), by taking line profiles in the three directions of high symmetry of the moiré and measuring the average peak-to-peak distance in each. The mean of those averages is 20.3 ± 0.7 Å, where the error is the error in the mean again. Alternatively it can be measured from the FFT of figure 2c) as 22 ± 2 Å, but this result is limited, because of the poor resolution of the spots, as the values change a lot per pixel near the center, due to it being reciprocal values. If it were a larger image, the moiré spots would be further from the center and better values could be achieved using FFT. These methods of calculating results and errors are used throughout the remainder of the chapter. The FFT method is preferred as it takes the whole image into account, instead of only the selected lines. The results achieved agree with the results reported by Ref. [9], where the atomic lattice and periodicity of the moiré are determined as 3.4 ± 0.3 Å and 20.7 Å, respectively. These values are the ones determined by STM in Ref. [9].

3.2 HOPG

The HOPG crystal consists of many layers of graphene. Therefore it was used to try and tune the evaporation parameters before using the BLG on SiC(0001) substrates, since only a limited number of those was available, and as mentioned earlier, the surface interaction is expected to be similar. The advantage of HOPG is that it can be reused many times however, as one can use a piece of scotch tape to cleave

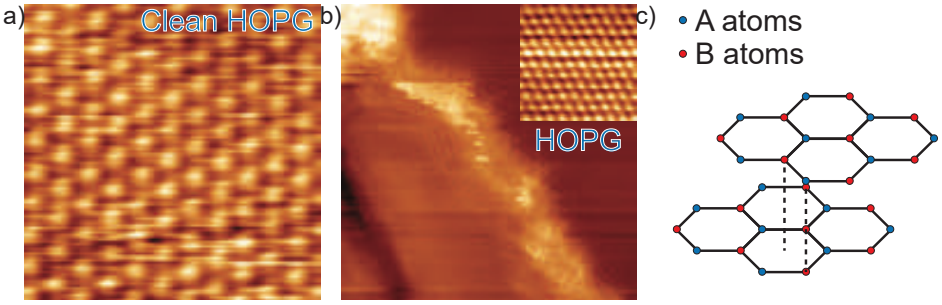

Figure 3: a) A $(24 \times 24)\,\text{Å}^2$ atomically resolved image of clean HOPG. This clearly shows the apparent hexagonal structure. Image parameters: $V_b = 18.6\,\text{mV}$ and $I_t = 1.0\,\text{nA}$ b) A $(133 \times 133)\,\text{Å}^2$ atomically resolved image of the HOPG after the last growth attempt. Note the change in structure around the large defect indicating an interaction between the evaporated material and the HOPG. The inset shows a $(24 \times 24)\,\text{Å}^2$ zoom from the upper right of the image, showing the similarity to the clean HOPG. Image parameters: $V_b = 582.6\,\text{mV}$ and $I_t = 1.0\,\text{nA}$ c) A model showing the AB stacking order of HOPG, which makes the lattice look hexagonal in STM images.

the substrate. By removing the top layers via sticking the tape to the surface and peeling it off, one obtains pristine HOPG beneath. Therefore this is the ideal substrate to test the growth parameters on before the graphene.

After cleaving, the HOPG substrate is cleaned by annealing it for 30 minutes at $\sim 300\,^\circ\text{C}$. An atomically resolved image of clean HOPG is shown in figure 3a). Three growth cycles were performed, inspired by the procedure set out by Ref. [15] for growing islands of SL MoS_2 on HOPG. This meant a 10 minute evaporation followed by a post-anneal at $\sim 730\,^\circ\text{C}$ for 60 minutes, at DMDS pressure of $\sim 5 \cdot 10^{-6}\,\text{mbar}$. It should be mentioned that because we had problems with the connection to the thermocouple at high temperatures (the connectors expand thermally, which can cause problems), the voltage across the filament

was simply set at 10.8 V, which results in around $\sim$ 730 °C, instead of controlling it via the temperature measured. The success of the attempts were evaluated qualitatively based on both large scale and close up STM images. The first attempt (I_{em} = 24 mA) had what seemed like too little material. Then we increased the emission current (I_{em} = 30 mA) and tried again. There was now too much material on the surface, so the HOPG was cleaved before the last attempt, where the emission current was adjusted to be in between the first and second (I_{em} = 28 mA). Now, as seen in figure 3b) there was evidence of the induced defects interacting with the surface, because of the different structure around the defect. Small patches were also found with what appeared to be weak semblances of order. Most importantly, the amount of material stuck to surface seemed to be good, as it was less than a full monolayer, but not too little.

Furthermore HOPG exemplified the relevance of stacking order for the appearance of a layered surface in STM. HOPG exhibits AB stacking order, schematically shown in figure 3c). This means that some atoms have a neighboring atom in the layer directly below theirs, and some do not. Atoms without a sublayer neighbor have a higher LDOS, so every second atom appears brighter than the others, resulting in an apparent hexagonal lattice [24, 25]. This hexagonal lattice parameter is measured by FFT as 2.49 $\pm$ 0.02 Å and from an FFT of the upper right corner of figure 3b) as 2.46 $\pm$ 0.02 Å. These agree with the expected theoretical value of 2.46 Å [15], and indicate that most of the material seen in 3b) is HOPG.

3.3 NbS_2 on bilayer graphene on SiC(0001)

SiC is a crystal, that when cut the right way, has a Si-terminated face (0001) and a C-terminated face ($000\bar{1}$). When annealed to very high temperatures, the Si evaporates first, leaving the C behind. The C then orders itself in the most favourable way, which is one or more layers of graphene. The first layer to form during annealing is a carbon layer called the buffer layer. This carbon layer is not graphene since every third C atom is still covalently bonded to the Si, also leaving most of the Si atoms with dangling bonds. The buffer layer's interaction with the Si-terminated face results in a complex $(6\sqrt{3}\times 6\sqrt{3})R30^\circ$ superstructure, which can also be reconstructed with a (6×6) hexagonal quasi unit cell. The notation gives the superstructure's unit cell as a multiple of a more basic surface unit cell, and the R indicates a rotation of the unit cell. These two are given relative to the Si surface unit cells. After the buffer layer, the next carbon layers to form are then proper graphene layers [26–29]. The buffer layer's superstructure should show up as a hexagonal pattern in STM images for BLG, reflecting the quasi unit cell. [30]. Two different types of defects are also expected. The type A defects, which are a type of atomic defects enclosed by a different superstructure ($(\sqrt{3}\times\sqrt{3})R30^\circ$ relative to the graphene unit cells), and type B defects which are tubular mounds, that do not perturb the atomic lattice [31].

The BLG on SiC substrates were cleaned by annealing them at 200 °C for 30 minutes. Figure 4a) shows a large scale image of the clean BLG on SiC(0001). The terraces originate from the SiC terraces

[28, 31], and for each substrate, they are observed to generally run in the same direction on that substrate. Upon closer inspection, the hexagonal superstructure from the interaction with the buffer layer can also be seen, as evident from the FFT inset from the upper right corner. Scattered across the image are also examples of both A and B defects.

The SiC terraces are sometimes bunched as can be seen in places in figure 4a) and close-up in 4b). However single terraces are also found in places. In the bottom of figure 4b) is what seems to be a type B defect. Figure 4c) shows the expected hexagonal atomic lattice, since BLG can exhibit AB stacking in the same way as HOPG does. It also shows a type A defect, where there FFT clearly shows the outer atomic dots and the inner dots rotated by 30° indicating the expected superstructure. From FFTs the atomic lattice parameter of the clean BLG on SiC(0001) could be determined as 2.54 ± 0.03 Å, and the superstructure's periodicity as 18.3 ± 0.3 Å, fitting well with the expected (6×6) quasi unit cell of the superstructure, as the Si-Si in SiC spacing is 3.08 Å [29]. The atomic lattice spacing also agrees with the expected value, which is 2.46 Å for free-standing graphene [29], which is the same as the HOPG lattice, as one might expect.

For growth on the graphene, the evaporator parameters were kept very similar to the last attempt on HOPG, but because a lower surface interaction was expected, the evaporation time was increased to 15 minutes. The post-anneal time is also increased to 90 minutes, with the filament voltage still at 10.8 V. During the post-anneal of the first attempt, it was decided to increase the DMDS pressure from $\sim 5 \cdot 10^{-6}$ mbar to $\sim 8 \cdot 10^{-6}$ mbar to hopefully increase the chances of

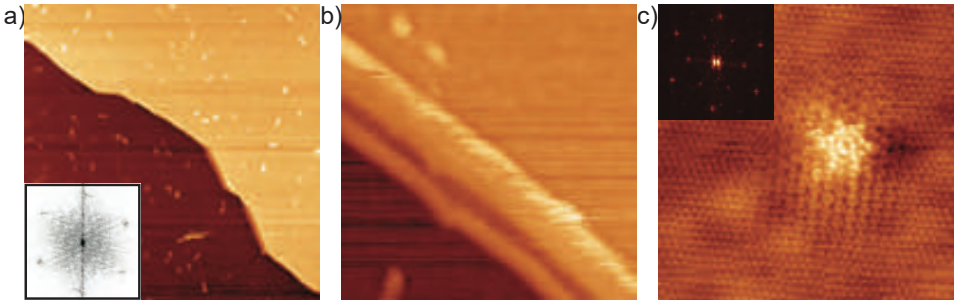

Figure 4: a) A (1359×1359) Å^2 STM image of clean graphene, showing a typical terrace running along one direction. Note the two places where it seems the terrace is doubled. The bright spots are defects, the round ones of which are A defects and the oblong ones of which are likely to be B defects. The inset shows the FFT of a close-up of the upper right corner, the dots indicating the hexagonal superstructure. The color scale has been inverted to show the dots more clearly. Image parameters: $V_b = 581.6\,\text{mV}$ and $I_t = 0.91\,\text{nA}$. b) A (272×272) Å^2 close-up of one of the double terraces clearly showing the structure of the edge. Image parameters: $V_b = 1240.2\,\text{mV}$ and $I_t = 0.57\,\text{nA}$. c) A (91×91) Å^2 atomically resolved image of the clean graphene, showing a well resolved type A defect and the hexagonal lattice structure. Note the apparent superstructure around the defect. The inset shows the center of the FFT the image, showing clear spots for the atomic lattice (the outer spots), and the differently rotated superstructure induced by the defect (the inner spots). Image parameters: $V_b = 1240.2\,\text{mV}$ and $I_t = 0.54\,\text{nA}$.

a reaction. Following the first attempt, we repeated the growth cycle with the same parameters as the first, but going to the higher DMDS pressure immediately. This second growth cycle seemingly resulted in larger islands, but because of a loose thermocouple, which induced noise in the STM, large scale images assessing island sizes, were not possible, and atomic resolution was not achieved. After the thermocouple was fixed, reproduction of the results was attempted on a new substrate, by adding the evaporation times of the first two attempts. However, the filament broke only 15 minutes into the post-anneal, re-

vealing that the anneal following the evaporation is essential to form nice islands, as there were only bright spots with no order. Since the filament could not be replaced without venting the chamber, there was not enough time to repeat the experiment. Therefore, all the results presented in figure 5 are from the same sample.

Comparing figure 4a) with figure 5a) it is clear that islands were formed by the growth cycle, and that some superstructure appears on them. The islands are nicely formed, consisting of mostly straight lines, and are mostly flat with some defects that are similar to those on the clean graphene. The island shapes are comparable to what is seen for NbS_2 on Au(111). The following investigation is then to determine what those islands are made of. For that purpose atomic resolution images were taken both off-island (figure 5b) and c)) and on-island (figure 5d) and e)). Off-island, we see a landscape very similar to the clean graphene, with A and B defects. Figure 5b) shows an atomically resolved image in which the (6×6) superstructure and a type A defect can be seen in the upper left corner. The hexagonal lattice structure is clear from the FFT, shown in the inset. The defect does not dominate the image enough to show up clearly in the FFT. The super structure can be seen in the FFT upon really close inspection of the center.

During the same scan of the sample, evidence of a change in stacking order was also found. This can be seen in figure 5c), as the seamless transition between the hexagonal structure in the bottom of the image to the honeycomb structure found in the top of the image. The seamless nature of the transition indicates that this is not the result of a tip change causing corrugation inversion. This change in stacking order has been observed before, and is proposed to be the product of

shifting the bottom graphene layer by a single SiC lattice vector [30]. Most of the sample exhibits AB stacking however.

On the islands, we see that we can achieve atomic resolution on the edges, and that neither the atomic lattice nor superstructure seemingly undergoes a large change going onto the island, as seen in figure 5d). Figure 5e) shows the atomic lattice on the island, alongside a representative FFT from another atomically resolved on-island image. Upon comparisons between on, and off-island FFTs from the same days, no evidence can be found of any relative rotation of the lattice, which would also have resulted in a rotation of the FFT.

In the end the off-island parameters for atomic lattice and superstructure are found. Using only figure 5b), the atomic lattice parameter is found to be 2.56 ± 0.07 Å. If one includes figure 5c) in the calculation the atomic lattice parameter is instead found as 2.59 ± 0.06 Å, where the difference most likely comes from the dominance of the change in stacking order seen in figure 5c), which seemingly affects the FFT. The lattice parameter for the superstructure is found as 18.7 ± 0.3 Å. On the islands, the parameters for atomic lattice and superstructure are measured as 2.53 ± 0.02 Å and 18.9 ± 0.2 Å. Hence there is seemingly no clear difference between the surface structure on and off the islands, and they both agree with the measurements of the clean BLG on SiC(0001) substrate. As mentioned earlier, rough estimates of island and terrace heights can be made from line profiles across edges, such as the one shown in figure 5f). From figure 4b) and another image not shown, that the single SiC terrace is 3.1 ± 0.2 Å while the island height, from figure 5a), d) and others, is 2.5 ± 0.2 Å. Clearly, there is a difference in the apparent height.

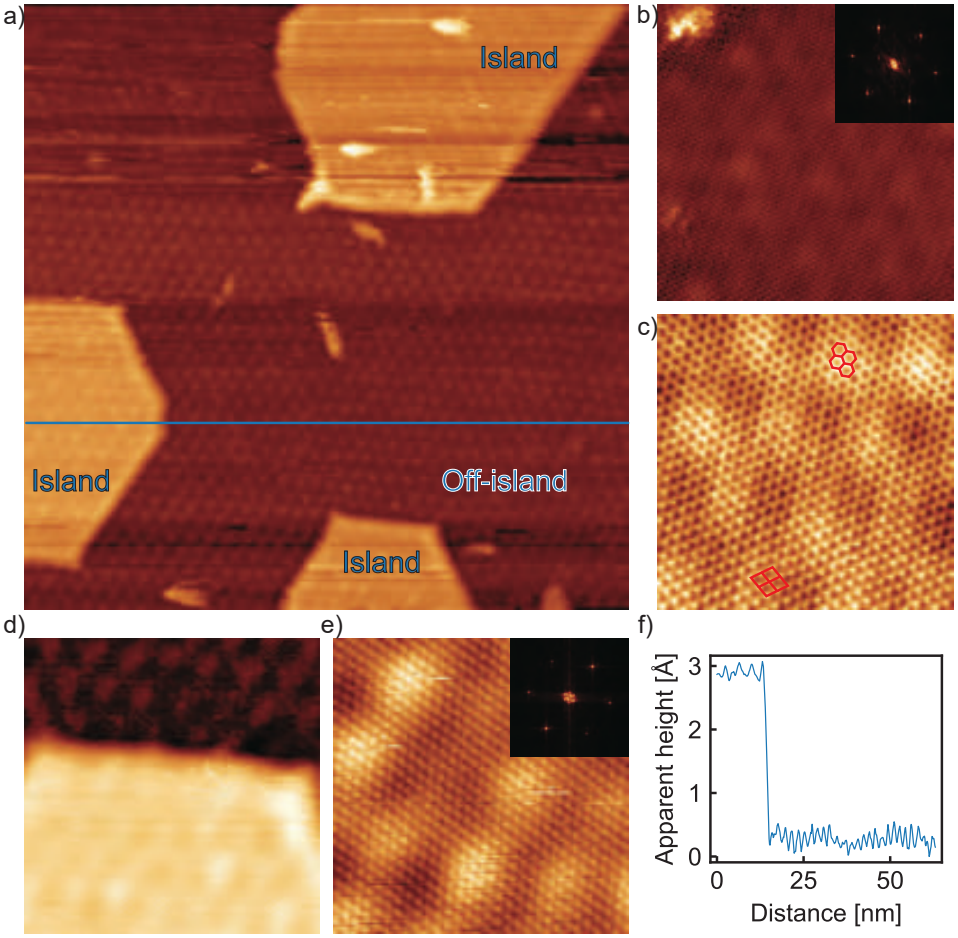

Figure 5: a) A $(636 \times 636)\,\text{Å}^2$ STM image showing examples of islands and the off-island region. Note the superstructure is present both on and off the islands. Image parameters: $V_b = 883.8\,\text{mV}$ and $I_t = 0.39\,\text{nA}$. b) A $(135 \times 135)\,\text{Å}^2$ atomically resolved image taken off-island. Note the defect in the corner, similar to figure 4c), and the dark hexagonal superstructure. The inset shows the FFT of the image, clearly indicating the hexagonal atomic lattice structure. Image parameters: $V_b = -110.5\,\text{mV}$ and $I_t = -0.13\,\text{nA}$. c) A close-up $(63 \times 63)\,\text{Å}^2$ atomically resolved image showing the two stacking orders, indicated by red, taken off-island. Image parameters: $V_b = -110.5\,\text{mV}$ and $I_t = -0.12\,\text{nA}$. d) A $(135 \times 135)\,\text{Å}^2$ image, taken at an island edge, clearly showing the superstructure both on and off the island. Image parameters: $V_b = 625.0\,\text{mV}$ and $I_t = 0.87\,\text{nA}$. e) A $(63 \times 63)\,\text{Å}^2$ atomically resolved image taken on and island, alongside an FFT of a similar image, showing a very similar atomic lattice to the off-island case. Image parameters: $V_b = 883.8\,\text{mV}$ and $I_t = 0.55\,\text{nA}$. f) Line profile from the blue line in a), showing the island height and corrugations from the superstructure.

4 Discussion

As shown in the section above, it appears something has happened to the substrate. The remaining question is what. STM is a chemically insensitive technique, meaning it cannot detect which element or compound it is scanning. This means that the chemical composition of the islands cannot be discovered directly from STM. Based on the successful growth of NbS_2 on Au(111) presented here, and the growth of many other TMDCs through similar methods, we may assume that the reaction between the Nb and DMDS can indeed take place with this method. Therefore it is likely, that it is some form of NbS_2 that makes up the islands. The question then becomes whether the NbS_2 is growing nicely on top of the graphene, as it does for Au(111), or if it is intercalated beneath the graphene layers.

The two scenarios are represented in figure 6a). If if were intercalated, one would expect to measure the BLG lattice on the islands, such that it closely resembles the off-island case. In the non-intercalated case one would expect to image the top layer of S atoms of the NbS_2, so that the lattice would be similar to what is seen on Au(111), but most likely with a different or no moiré, as the graphene lattice is different, and the buffer layer superstructure is also there. As the lattice measurements on and off the islands are very similar for both the atomic lattice and the superstructure, the intercalated case is more likely.

The similarity between the on and off-island lattices also leaves the possibility that, some step of the growth process, for example the anneal, simply creates islands of more layers of graphene. There are

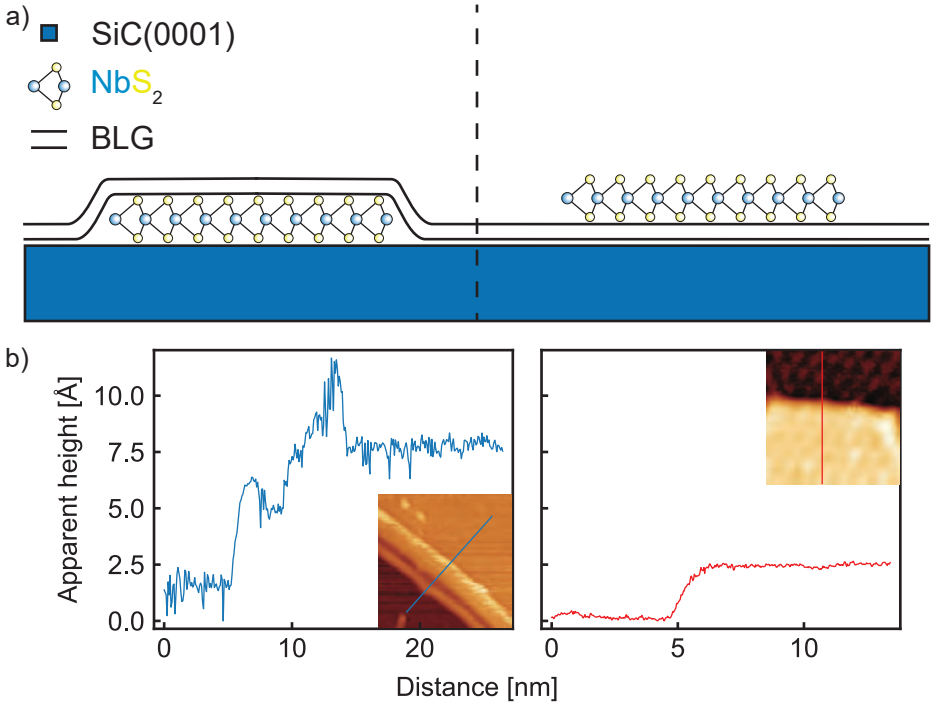

Figure 6: a) A simple model showing the two likely scenarios for NbS_2 on BLG on SiC(0001) (shown here is the trigonal prismatic phase). Left: The NbS_2 is intercalated beneath both layers of graphene. Right: The NbS_2 is atop the BLG. b) Left: A line profile, shown in blue on the the image in the inset, see 4b), showing the heights of the individual and double terrace. Right: A line profile shown in red on the inset, see figure 5d), showing the island height.

methods of determining number of graphene layers through STM, as seen in Ref. [30], through a statistical parameter called roughness, but since multiple samples of different known layer thicknesses were not available, we could not do any sort of calibration to determine the relation on the STM used, and therefore it would be nigh impossible to see whether it was two or three layers of graphene, or if maybe a slight change in roughness was induced by something else. One could also try to do a form of scanning tunneling spectroscopy (STS) with the STM, to measure the electronic structure or work function indicating

if it was just graphene, or if there was any trace of NbS_2. This was beyond the scope of this project however. Furthermore, based on Ref. [30], the clear buffer layer superstructure that is observed on top of the islands, would not be seen for 3 layers of graphene.

Another line of evidence to consider are the island heights. In figure 6b) there is a clear comparison between an island edge and the edges found on clean BLG on SiC. The average island height found is less than the average single SiC terrace, as mentioned earlier, indicating they are not a type of previously unobserved SiC terrace. Regarding the extra layer of graphene, one would then expect the step-height to match with the interlayer spacing of graphene (3.55 Å [30]), but again the values disagree. Comparison can be made with the work in Ref. [10], where SL NbS_2 was grown at much lower temperatures, probably making intercalation less likely, and where the lattice parameter matches the expected bulk value of 3.3 Å, meaning that the NbS_2 is most likely not intercalated. The island height measured (5.78 Å) is much closer to the bulk layer spacing (about 6.5 Å [32]), and also similar to the spacing between the SL and the BL NbS_2 measured in Ref. [9] (6.1 ± 0.2 Å) and Ref. [10] (5.99 Å). The similarity between the SL height on graphene and the layer spacing in the bulk version, results from the layers only being bonded by weak van der Waals forces in both cases. This indicates that the material that makes up the islands here, is not bonded by the van der Waals interaction, but some stronger force instead. Such a force might come from the dangling Si bonds, that any intercalated material might interact with.

Finally, if there is something intercalated, which seemingly is the case, the material might not even be NbS_2. It could simply be metal-

lic Nb, or perhaps a mixture of Nb and S. It could even be NbS_2, but unordered for some reason. A mass of unordered material might be probable since, if there was another ordered lattice beneath the graphene, one might expect to see a different moire and not the buffer layer superstructure. Unfortunately, it does not seem that any experimental work has been done, investigating graphene on TMDC systems, so there is nothing to compare the islands to in this regard. On the other hand, the well-formed islands indicate that it might be an ordered compound. Given the success of the growth method on Au(111), and the similarity in the shapes of the islands, the most likely seems to be ordered NbS_2. However, this is not a guarantee, and something unlikely might be happening. Again, this raises the point that more chemically sensitive techniques are needed, and the results presented here need to be reproduced, to ensure that the growth is deliberate.

5 Conclusion

SL NbS_2 was successfully grown on Au(111) and the results agree with the previously published work presented in Ref. [9]. SL Nb_S was not grown on HOPG, but through the experiments with HOPG, better evaporation parameters for growth on BLG on SiC(0001) were found. Lastly an attempt was made to grow SL NbS_2 on BLG on SiC(0001), however the result is unclear. It seems highly probable that some material has intercalated beneath the BLG, forming well-shaped, flat islands, due to the surface structure remaining unchanged on the islands, and the island heights indicating an interaction stronger than a van der Waals bond, as they do not match the step heights

found for NbS_2 grown on BLG on SiC(0001). Furthermore the island heights also indicate that they are not SiC terraces, nor an extra layer of graphene, the last case also being unlikely due to the persistance of the superstructure on the islands. The shapes of the islands indicate that it might be some ordered structure, and given the similarity of both method and resulting shapes to the successful growth on Au(111), it seems likely that the intercalated material is some form of NbS_2.

5.1 Outlook

As mentioned earlier, a more chemically sensitive technique is needed to determine for certain what the intercalated material is. One such technique could be X-ray photoemission spectroscopy (XPS). As the name suggests this uses high energy photons in the X-ray region to photoexcite the core level electrons. The electrons emitted can be recorded by a spectrometer, and by energy conservation the binding energy can be found. The core level electrons act as elemental indicators, so by analysing XPS spectra, where there are peaks at the occupied core energy levels, one can figure out which elements are present in the sample [9]. If it turns out that there are traces of elemental Nb and S, one could also use the XPS spectra to analyse the chemical environment around the Nb and S to determine if the material is on top of the graphene or intercalated. If one could then obtain high enough island coverage, one could move on to use angle resolved photoemission spectroscopy (ARPES) to measure the electronic structure of the valence band electrons to see if there is any trace of NbS_2.

Atomic force microscopy (AFM) could also be used to acquire more

accurate measurements of the island heights. AFM is similar to STM, but instead of measuring the tunneling current, AFM measures the force between the atoms to obtain images of the surface [33, 34]. AFM therefore results in a direct height measurement, rather than the apparent height measured by STM, which is a convolution of the LDOS and topography.

Overall, this seems like a very promising line of research, in which there is still much left to do. If success is found, this material could prove an interesting platform for all sorts of fascinating effects. As mentioned NbS_2 on BLG on SiC already shows a CDW not present on Au(111) or in the bulk version, but perhaps NbS_2 grown by a different method will show other properties, and have the potential to reveal new and interesting information.

6 References

[1] M. Chhowalla, H. S. Shin, G. Eda, L.-J. Li, K. P. Loh, and H. Zhang. The chemistry of two-dimensional layered transition metal dichalcogenide nanosheets. *Nature Chemistry*, 5(4):263–275, 2013.

[2] S. Das, J. A. Robinson, M. Dubey, H. Terrones, and M. Terrones. Beyond Graphene: Progress in Novel Two-Dimensional Materials and van der Waals Solids. *Annual Review of Materials Research*, 45(1):1–27, 2015.

[3] W. Choi, N. Choudhary, G. H. Han, J. Park, D. Akinwande, and Y. H. Lee. Recent development of two-dimensional transition metal dichalcogenides and their applications. *Materials Today*, 20(3):116–130, 2017.

[4] J. Shi, M. Hong, Z. Zhang, Q. Ji, and Y. Zhang. Physical properties and potential applications of two-dimensional metallic transition metal dichalcogenides. *Coordination Chemistry Reviews*, 376:1–19, 2018.

[5] M. Naito and S. Tanaka. Electrical Transport Properties in 2H-NbS_2, -$NbSe_2$, -TaS_2 and -$TaSe_2$. *Journal of the Physical Society of Japan*, 51(1):219–227, 1982.

[6] I. Guillamón, H. Suderow, S. Vieira, L. Cario, P. Diener, and P. Rodière. Superconducting Density of States and Vortex Cores of 2H-NbS_2. *Phys. Rev. Lett.*, 101:166407, 2008.

[7] C. Heil, S. Poncé, H. Lambert, M. Schlipf, E. R. Margine, and F. Giustino. Origin of Superconductivity and Latent Charge Density Wave in NbS_2. *Phys. Rev. Lett.*, 119:087003, 2017.

[8] P. Dreher, W. Wan, A. Chikina, M. Bianchi, H. Guo, R. Harsh, et al. Proximity Effects on the Charge Density Wave Order and Superconductivity in Single-Layer $NbSe_2$. *ACS Nano*, 15(12):19430–19438, 2021.

[9] R.-M. Stan. *Epitaxial growth of single-layer metallic transition metal dichalcogenides: Structural and electronic properties*. Ph.D. Department of Physics and Astronomy, Aarhus University, 2019.

[10] H. Lin, W. Huang, K. Zhao, C. Lian, W. Duan, X. Chen, et al. Growth of atomically thick transition metal sulfide films on graphene/6H-SiC(0001) by molecular beam epitaxy. *Nano Research*, 11(9):4722–4727, 2018.

[11] C. E. Sanders, M. Dendzik, A. S. Ngankeu, A. Eich, A. Bruix, M. Bianchi, et al. Crystalline and electronic structure of single-layer TaS_2. *Phys. Rev. B*, 94:081404, 2016.

[12] P. Hofmann. *Solid State Physics: An Introduction*. Wiley-VCH Berlin, 2nd edition, 2015.

[13] V. S. Smentkowski. Trends in sputtering. *Progress in Surface Science*, 64(1):1–58, 2000.

[14] P. M. Spurgeon, K. C. Lai, Y. Han, J. W. Evans, and P. A. Thiel. Fundamentals of Au(111) Surface Dynamics: Coarsening of Two-Dimensional Au Islands. *Journal of Physical Chemistry. C*, 124(13), 2020.

[15] J. Kibsgaard. *Atomic-scale investigation of MoS_2-based hydrotreating model catalysts. A scanning tunneling microscopy study.* Ph.D. Interdisciplinary Nanoscience Center (iNANO), Department of Physics, and Astronomy, Aarhus University, 2008.

[16] S. S. Grønborg, S. Ulstrup, M. Bianchi, M. Dendzik, C. E. Sanders, J. V. Lauritsen, et al. Synthesis of Epitaxial Single-Layer MoS_2 on Au(111). *Langmuir*, 31(35):9700–9706, 2015.

[17] G. Binnig and H. Rohrer. Scanning tunneling microscopy. *Surface Science*, 126(1):236–244, 1983.

[18] C. J. Chen. *Introduction to Scanning Tunneling Microscopy: Second Edition.* Oxford University Press, 2008.

[19] J. Tersoff and D. R. Hamann. Theory of the scanning tunneling microscope. *Phys. Rev. B*, 31:805–813, 1985.

[20] I. Horcas, R. Fernández, J. M. Gómez-Rodríguez, J. Colchero, J. Gómez-Herrero, and A. M. Baro. WSxM : A software for scanning probe microscopy and a tool for nanotechnology. *Review of Scientific Instruments*, 78(1):013705, 2007.

[21] C. Wöll, S. Chiang, R. J. Wilson, and P. H. Lippel. Determination of atom positions at stacking-fault dislocations on Au(111) by scanning tunneling microscopy. *Phys. Rev. B*, 39:7988–7991, 11, 1989.

[22] J. V. Barth, H. Brune, G. Ertl, and R. J. Behm. Scanning tunneling microscopy observations on the reconstructed Au(111) surface: Atomic structure, long-range superstructure, rotational domains, and surface defects. *Phys. Rev. B*, 42:9307–9318, 1990.

[23] K. Hermann. Periodic overlayers and moiré patterns: theoretical studies of geometric properties. *Journal of Physics: Condensed Matter*, 24(31):314210, 2012.

[24] R. C. Tatar and S. Rabii. Electronic properties of graphite: A unified theoretical study. *Phys. Rev. B*, 25:4126–4141, 1982.

[25] I. P. Batra, N. García, H. Rohrer, H. Salemink, E. Stoll, and S. Ciraci. A study of graphite surface with stm and electronic structure calculations. *Surface Science*, 181(1):126–138, 1987.

[26] T. Seyller, A. Bostwick, K. V. Emtsev, K. Horn, L. Ley, J. L. McChesney, et al. Epitaxial graphene: a new material. *physica status solidi (b)*, 245(7):1436–1446, 2008.

[27] K. V. Emtsev, F. Speck, T. Seyller, L. Ley, and J. D. Riley. Interaction, growth, and ordering of epitaxial graphene on SiC(0001) surfaces: A comparative photoelectron spectroscopy study. *Phys. Rev. B*, 77:155303, 2008.

[28] J. Baringhaus. *Mesoscopic transport phenomena in epitaxial graphene nanostructures: A surface science approach.* Ph.D. Fakultät für Mathematik und Physik der Gottfried Wilhelm Leibniz Universität Hannover, 2015.

[29] G. R. Yazdi, T. Iakimov, and R. Yakimova. Epitaxial Graphene on SiC: A Review of Growth and Characterization. *Crystals*, 6(5), 2016.

[30] P. Lauffer, K. V. Emtsev, R. Graupner, T. Seyller, L. Ley, S. A. Reshanov, et al. Atomic and electronic structure of few-layer graphene on SiC(0001) studied with scanning tunneling microscopy and spectroscopy. *Phys. Rev. B*, 77:155426, 2008.

[31] Q. Wang, W. Zhang, L. Wang, K. He, X. Ma, and Q. Xue. Large-scale uniform bilayer graphene prepared by vacuum graphitization of 6H-SiC(0001) substrates. *Journal of Physics: Condensed Matter*, 25(9):095002, 2013.

[32] A. Kuc, T. Heine, and A. Kis. Electronic properties of transition-metal dichalcogenides. *MRS Bulletin*, 40(7):577–584, 2015.

[33] G. Binnig, C. F. Quate, and C. Gerber. Atomic Force Microscope. *Phys. Rev. Lett.*, 56:930–933, 1986.

[34] F. J. Giessibl. Atomic Resolution of the Silicon (111)-(7×7) Surface by Atomic Force Microscopy. *Science*, 267(5194):68–71, 1995.